© 2022. Published by The Company of Biologists Ltd | Development (2022) 149, dev200415. doi:10.1242/dev.200415

TECHNIQUES AND RESOURCES

RESEARCH ARTICLE

Fluorescent cytoskeletal markers reveal associations between the actin and microtubule cytoskeleton in rice cells

Zengyu Liu[1], Isabella Østerlund[2,3], Felix Ruhnow[2], Yiran Cao[1], Guoqiang Huang[1], Wenguo Cai[1], Jiao Zhang[1], Wanqi Liang[1], Zoran Nikoloski[3], Staffan Persson[1,2,4,*] and Dabing Zhang[1,5,*]

ABSTRACT

Rice (*Oryza sativa*) is one of our main food crops, feeding ~3.5 billion people worldwide. An increasing number of studies note the importance of the cytoskeleton, including actin filaments and microtubules, in rice development and environmental responses. Yet, reliable *in vivo* cytoskeleton markers are lacking in rice, which limits our knowledge of cytoskeletal functions in living cells. Therefore, we generated bright fluorescent marker lines of the actin and microtubule cytoskeletons in rice, suitable for live-cell imaging in a wide variety of rice tissues. Using these lines, we show that actin bundles and microtubules engage and co-function during pollen grain development, how the cytoskeletal components are coordinated during root cell development, and that the actin cytoskeleton is robust and facilitates microtubule responses during salt stress. Hence, we conclude that our cytoskeletal marker lines, highlighted by our findings of cytoskeletal associations and dynamics, will substantially further future investigations in rice biology.

KEY WORDS: Cytoskeleton, Actin, Microtubule, Fluorescent markers, Live-cell imaging, Rice

INTRODUCTION

Rice (*Oryza sativa*) is one of the staple food crops for billions of people around the world (Seck et al., 2012). Understanding the response mechanisms of rice to diverse intra- and extra-cellular signals is tightly linked to improvements of rice performance. The plant cytoskeleton, composed of filamentous actin and microtubules, critically supports plant development and stress resistance in plants (Kost et al., 1999; Wang and Mao, 2019), including rice. Although most plant cytoskeleton studies have been performed in the model dicot plant *Arabidopsis thaliana*, there are also a few studies that highlight the importance of the cytoskeleton in rice development and environmental responses. For example, both actin- and microtubule-related rice mutants display severe developmental defects (Komorisono et al., 2005; Zhang et al., 2010), microtubule-related proteins were frequently reported to control rice seed size (Sun et al., 2017; Yang et al., 2020), and several rice cytoskeleton proteins were found to impact stress resistance (Xu et al., 2018; Lo et al., 2020). Therefore, it is important to study the cytoskeleton in detail in rice.

Most of the rice cytoskeleton reports focus on mutant characterization, with negligible *in vivo* cytoskeleton investigations (Zhang et al., 2010; Li et al., 2014; Huang et al., 2018; Song et al., 2019; Lo et al., 2020; Chang et al., 2021). In particular, important processes in rice, including tillering, underwater growth, pollen development and seed quality, have not yet been studied in connection with the cytoskeleton despite its prominent roles in these processes. Whereas static studies by immunolabelling are dominating the rice cytoskeleton field, live-cell imaging is superior because the cytoskeleton is composed of highly dynamic structures (Shaw et al., 2003; Sheahan et al., 2004). To this end, bright and stable fluorescent markers of the cytoskeleton are much needed. However, fluorescent cytoskeleton marker lines have only been established in some plant species, e.g. *Arabidopsis*, *Medicago* (*Medicago truncatula*), maize (*Zea mays*) and cotton (*Gossypium* spp.) (Shaw et al., 2003; Timmers et al., 2007; Mohanty et al., 2009; Yu et al., 2019). These studies have highlighted the importance of selecting suitable fluorescent tags and cytoskeleton-labelling proteins to minimize their influence on cytoskeletal behaviour and allow long-term visualization of the cytoskeletal structures (Sheahan et al., 2004). The fine Actin-Binding Domain 2 of *Arabidopsis* fimbrin 1 (fABD2), mTalin and Lifeact are commonly used for actin labelling (Kost et al., 1998; Sheahan et al., 2004; Qu et al., 2017), while tubulin subunits and the mammalian Microtubule-Associated Protein 4 (MAP4) are typical proteins for microtubule labelling (Marc et al., 1998; Ueda et al., 1999; Shaw et al., 2003). Notably, these labelling proteins may impact the behaviour of the cytoskeletons, and so the protein abundance and biochemical properties of marker proteins are important factors to consider (Courtemanche et al., 2016). However, the impacts of the marker proteins appear to differ among different organisms. That may be the reason why one construct performs well in one species or tissue, but not in another (Vidali et al., 2009; Flores et al., 2019), emphasizing the need to choose suitable components to construct markers for specific plants or tissues.

In this study, we generated effective rice fluorescent cytoskeleton marker lines, including those of filamentous actin and microtubules, allowing live-cell imaging of the rice cytoskeleton. With our marker lines, we explored several cytoskeleton-related topics in rice biology, including actin and microtubule interplay during pollen development and root cell division, salt response and cytoskeletal mutant characterization. We thus describe several exciting phenomena, which will open up further investigations on rice cytoskeleton functions.

[1]Joint International Research Laboratory of Metabolic and Developmental Sciences, School of Life Sciences and Biotechnology, Shanghai Jiao Tong University, Minhang 200240, Shanghai, China. [2]Department of Plant and Environmental Sciences (PLEN), University of Copenhagen, 1870 Frederiksberg, Denmark. [3]Systems Biology and Mathematical Modelling, Max Planck Institute of Molecular Plant Physiology, Am Mühlenberg 1, 14476 Potsdam-Golm, Germany. [4]Copenhagen Plant Science Center (CPSC), University of Copenhagen, 1870 Frederiksberg, Denmark. [5]School of Agriculture, Food, and Wine, University of Adelaide, Waite Campus, Urrbrae, SA 5064, Australia.

*Authors for correspondence (zhangdb@sjtu.edu.cn; staffan.persson@plen.ku.dk)

Z.L., 0000-0002-8784-2045; Y.C., 0000-0002-3707-1238; Z.N., 0000-0003-2671-6763; D.Z., 0000-0003-3181-9812

Handling Editor: Ykä Helariutta
Received 3 December 2021; Accepted 9 May 2022

Development (2022) 149, dev200415. doi:10.1242/dev.200415

RESULTS

Generation of cytoskeleton markers in rice

To study cytoskeletal dynamics in rice *in vivo*, we set out to generate fluorescent marker lines for the microtubule and actin cytoskeleton. We generated a range of different combinations of promoters, fluorescent proteins and cytoskeleton-labelling proteins (Fig. 1). We transformed these into wild-type rice plants and screened multiple independent transgenic lines in T2 generation. The advantages and disadvantages of these tested components are compared and summarized in Table S1. We found that the monocot ubiquitin promoters including rice ubiquitin 2 (*RUBQ*) and maize ubiquitin 1 (*Ubi1*) gave homogeneous fluorescent signals in rice cells, while the tobacco virus promoter 35S was often silenced (Fig. 1A,B). *RUBQ* lines typically showed brighter signals than *Ubi1*-driven lines. Inspired by Arabidopsis studies, we tried the domain of mouse MAP4 and the rice Tubulin subunit Alpha 1 (OsTUA1) to label rice microtubules, and Arabidopsis actin-binding protein fABD and its rice homolog OsfABD to label rice actin filaments. In the resulting transgenic lines, OsTUA1 labelled rice microtubules weakly, but substantial fluorescence was also observed in the cytosol (see white arrowheads in Fig. 1B). No signal was detected in the OsfABD lines (second image in Fig. 1A). Fortunately, MAP4 and fABD lines effectively labelled the microtubule and actin cytoskeleton in rice plants (right three columns in Fig. 1A,B). Notably, fABD lines were developmentally indistinguishable from wild-type plants, whereas the MAP4 lines occasionally caused some growth defects also reported for different microtubule marker lines in Arabidopsis (Fig. S1A). However, wild-type-like MAP4 transgenic lines were also frequently obtained (Fig. S1B). Among the fluorescent proteins we used, the bright green fluorescent protein mNeongreen (mNG) appeared bright and stable, while the red fluorescent protein mScarlet was bright but prone to photo-bleaching (Fig. S1C,D).

We first visualized the cytoskeleton throughout different rice tissues, including roots, root hairs, stem, leaves, stomata, anthers, pollen grains and pollen tubes (Fig. 2A,B). Bright fluorescence was observed in all tissues, except in the pollen mother cell before microspore formation (Fig. S2). Overall, we observed brighter fluorescence in younger plant tissues. Thus, our marker lines can be used to image the organization and dynamic behaviour of the cytoskeleton in both vegetative and reproductive tissues (Fig. 2C,D, Movies 1, 2), including cells with different growth modes.

Live-cell imaging reveals dramatic reorganization of the cytoskeleton during rice pollen development

Using our marker lines, we set out to explore a range of processes related to the cytoskeletons. We first imaged cytoskeletal behaviour during rice pollen development. As shown in Fig. 3, both the actin and microtubule cytoskeletons were fragmented in young microspores (left column). Short actin filaments and microtubules subsequently formed during pollen grain development (bright-field panels from left to right in Fig. 3). Both actin filaments and microtubules gradually extended as the pollen grains increased in size; however, the polymers lacked clear common directionality. During pollen grain maturation and amyloplast formation (red asterisks in Fig. 3), both the actin and microtubule cytoskeletons formed radial patterns radiating from the germination pore (indicated by yellow arrows in Fig. 3). Once the pollen was hydrated, the cytoskeleton gradually became disordered again and partially depolymerized (right column in Fig. 3).

The radial alignment of the actin and microtubule cytoskeletons prompted us to consider whether the two structures perhaps function together and associate with each other. Therefore, we obtained actin and microtubule cytoskeleton dual-labelled lines (*RUBQ::mNG-fABD* and *RUBQ::mScarlet-MAP4*) by crossing the single marker lines. In the resulting lines, we observed bright fluorescence from

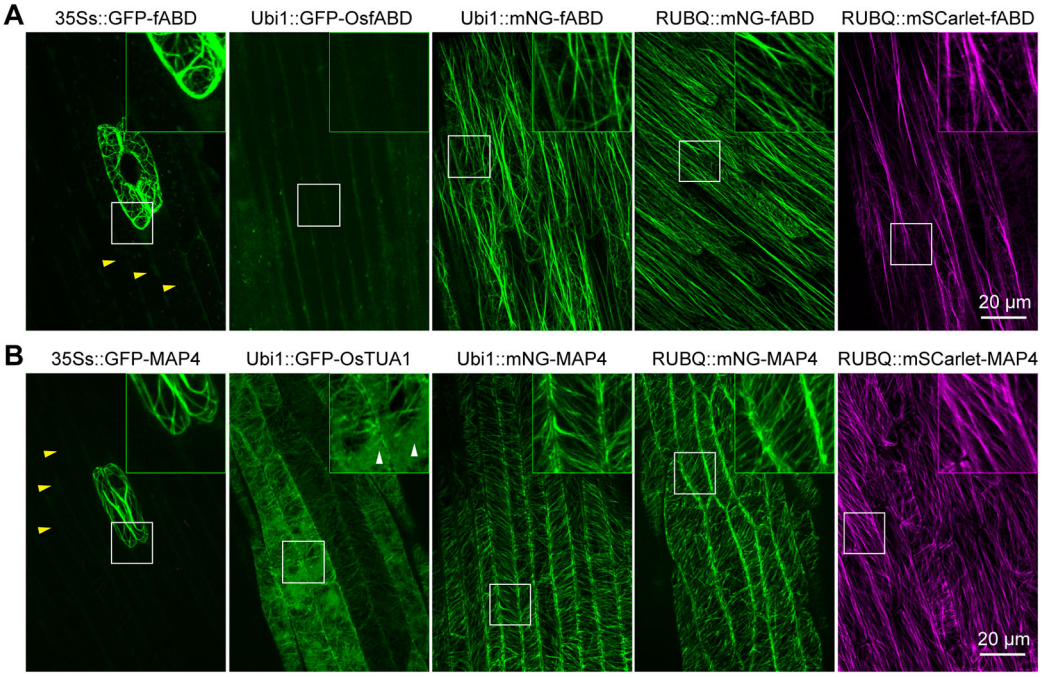

Fig. 1. Comparison of different rice cytoskeleton marker lines. (A,B) Actin (A) and (B) microtubule cytoskeleton markers in transgenic rice coleoptile. Epidermises of coleoptiles, germinated for 3.5 days, were used for the imaging. The images are maximum projections from *z*-stack series. The white boxes indicate the regions for enlargement in the upper-right corner in images. The yellow arrowheads indicate cells with silenced signals and the white arrowheads indicate cytosolic signals.

Development (2022) 149, dev200415. doi:10.1242/dev.200415

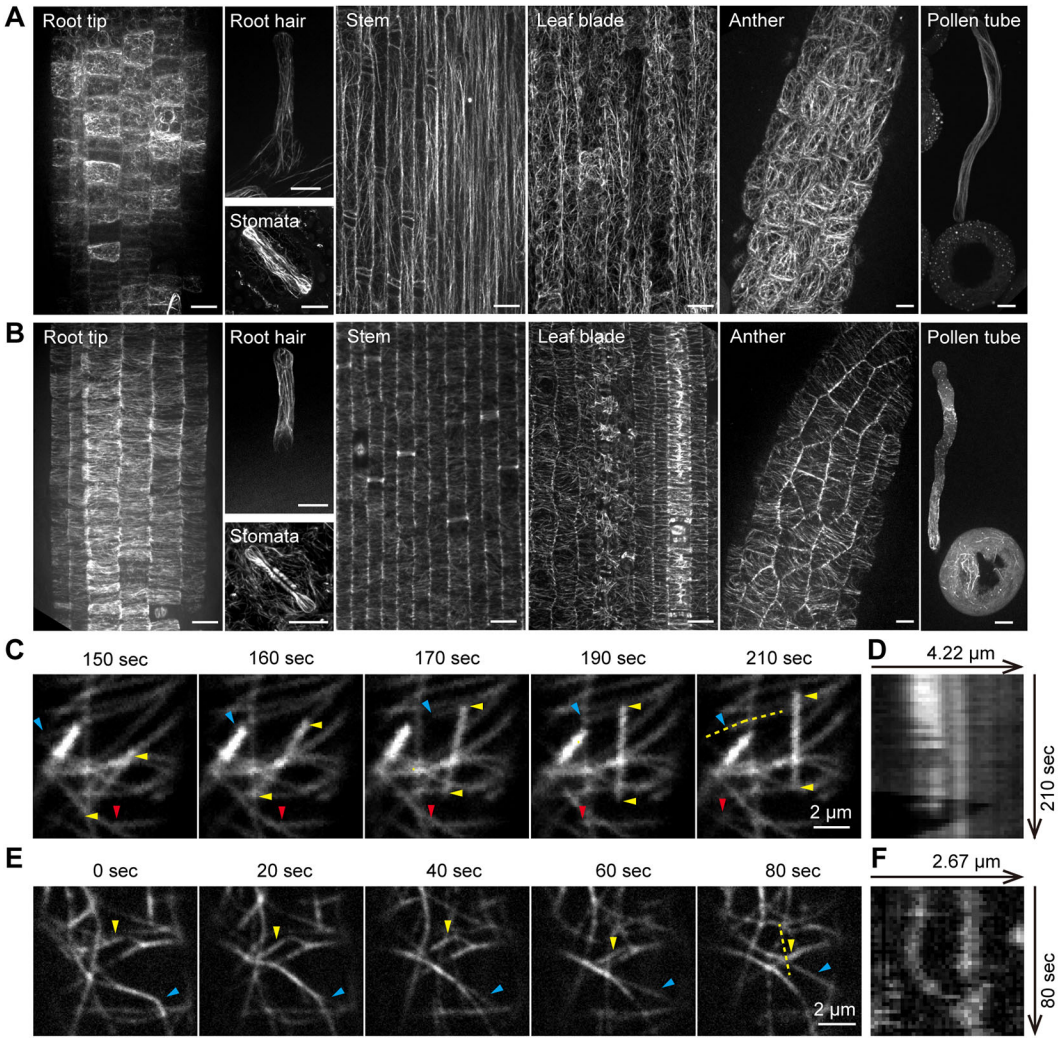

Fig. 2. Cytoskeletal patterns and behaviour in different rice tissues shown using live-cell imaging of fluorescent marker lines. (A) Example images of actin cytoskeleton in different rice tissues, including vegetative cells and reproductive cells. All images are maximum projections and obtained from the actin line *RUBQ::mNG-fABD* (mNG-fABD). Scale bars: 10 µm. (B) Example images of microtubules in different rice tissues. The images of the root tip and root hair were obtained from *RUBQ::mScarlet-MAP4* (mScarlet-MAP4 hereafter) lines; all other images were from the *RUBQ::mNG-MAP4* (mNG-MAP4) line. All images are maximum projections. Scale bars: 10 µm. (C) A time series of mNG-MAP4 in root with 5 s time interval. The yellow, red and blue arrowheads are following a treadmilling microtubule, a growing microtubule end and a catastrophe microtubule, respectively. (D) Kymograph following the microtubule catastrophe. The position is indicated by the dashed line in C. (E) A time series of mNG-fABD in root with 2 s time interval. The yellow and blue arrowheads are following a bundling and unbundling actin filament and bundle, respectively. (F) Kymograph following the bundling actin event at the position indicated by the dashed line in E.

both markers and subsequently observed actin and microtubule cytoskeletons simultaneously in mature pollen grains. Strikingly, we found that the two fluorescent signals overlapped (Fig. 4A,B). Indeed, the two markers showed 70% colocalization based on Pearson correlation coefficient analyses (Fig. 4C). Closer observations revealed that thick actin bundles radiated out from the germination pores (indicated by the white arrowheads in Fig. 4D), whereas filamentous actin interspersed these bundles (indicated by the yellow arrowheads in Fig. 4D). Interestingly, the colocalization of actin and microtubule cytoskeleton occurred along the actin bundles, and not the fine filaments (as shown in Fig. 4D and Movie 3). This is consistent with colocalization analyses using Mander's coefficient test, in which up to 90% of the microtubule-related fluorescence colocalized with the fluorescence from the actin cytoskeleton, whereas only ∼50% of the actin-related fluorescence colocalized with the microtubule signal (Fig. 4C).

To address whether the two cytoskeletal structures are associated with each other in mature pollen grains, we recorded time-lapse imaging of the dual-labelled line. Here, we found that the microtubules were coordinated with the actin bundles (Fig. 4E,F), indicating a tight interplay between the two cytoskeletal structures. This indicated that there may be a mutual structural and perhaps a functional relationship between the cytoskeletal components in pollen grains. We investigated this by disrupting one of the polymers and observed whether this resulted in any changes in the other one. When the actin cytoskeleton was partially depolymerized by actin inhibitor latrunculin B, the number of microtubule polymers did not obviously change (Fig. 4G, Movie 4). However, the microtubule radial organization was perturbed and the engagement with actin decreased, i.e. the Pearson correlation coefficient between the microtubules and the remaining actin filaments was reduced (Fig. 4G, Fig. S3). Notably, when the microtubules were depolymerized using oryzalin, the radial actin bundles rapidly disappeared and were replaced by a myriad of cytosolic actin filaments (Fig. 4H, Movie 5). Overall, the oryzalin treatment was accompanied by a reduction in actin filamentous

Development (2022) 149, dev200415. doi:10.1242/dev.200415

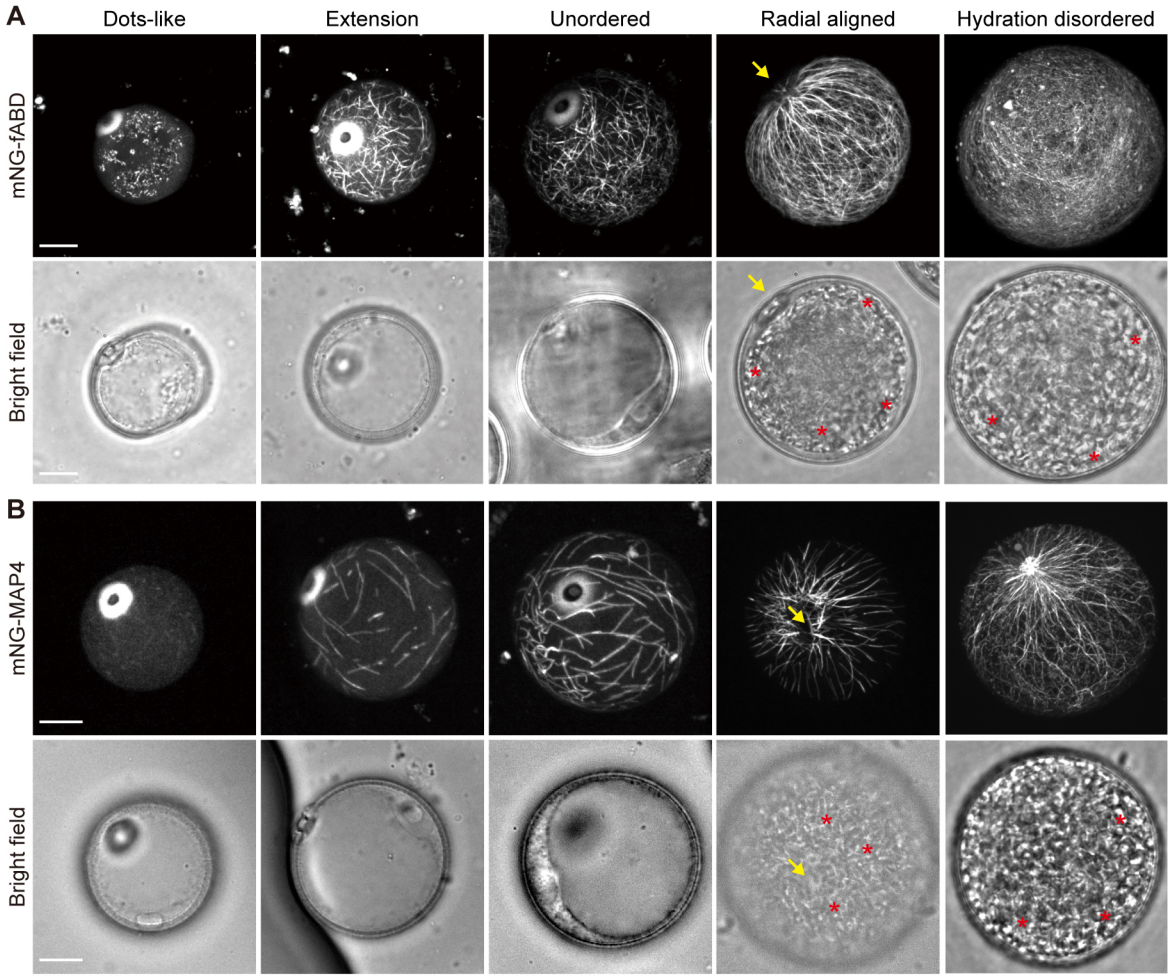

Fig. 3. Organizational changes in the cytoskeleton during rice pollen development. (A) Actin filament organization at different pollen developmental stages. (B) Microtubule organization at different pollen developmental stages. The fluorescent channels are maximum projections of *z*-stacks. The bright-field channels are a single focal plane selected from *z*-stacks to show the size of the pollen. The diameter increase (from left to right) of the pollen grains indicates development of the pollen from immature to mature. The pollen germination pores are indicated by the yellow arrows. The red asterisks indicate amyloplasts. Scale bars: 10 µm.

fluorescence (middle column in Fig. 4H). These observations indicate that the actin and microtubule cytoskeleton provide mutual structural support to each other during pollen grain development.

Actin and microtubule array reorganization in root cells of rice

Motivated by the cytoskeletal interactions in rice pollen, we next examined their relationship in other cell types, such as root cells. Here, microtubules play an essential role during cell division and display distinct configurations at different division stages, including preprophase band, spindle and phragmoplast (Lipka et al., 2015). These configurations were also clearly observed in dividing rice root cells by our marker lines (Fig. 5). Actin filaments function in cell division (Maeda et al., 2020); however, the actin configurations during cell division remain controversial (Panteris, 2008). In rice root cells, the abundant actin filaments in non-dividing cells gradually disappeared during preprophase band formation (Fig. 5). At telophase, we detected scant actin cytoskeletal fluorescence (Fig. 5). However, we noted clear actin-related fluorescence during phragmoplast progression (indicated by the arrowhead in Fig. 5), where the fluorescence appeared to be associated with the emerging cell plate. This observation is consistent with the reported cell plate-promoting function of actin cytoskeleton (Maeda and Higaki, 2021). Hence, in contrast to in the pollen grains, the actin and microtubule cytoskeletons appear to function separately in dividing rice root cells. The disappearance of the actin cytoskeleton may coincide with reduced cytoplasmic streaming, which decreases during the onset of division in *Paramecium bursaria* (Sikora et al., 1991).

In interphase rice root cells, we did not detect any obvious association between the actin and microtubule cytoskeletons (Fig. 6A). As reported in Arabidopsis, transverse microtubule arrays in elongating root cells re-arrange towards a longitudinal direction during cell maturation and growth cessation (Chan, 2012; Adamowski et al., 2019). We also noted a similar re-orientation in developing rice roots (top row in Fig. 6A). Interestingly, we also found a similar re-organization of the actin cytoskeleton (bottom row in Fig. 6A). To quantify such change, we extracted filament edge angles using the Cytoseg2.0 algorithm (Nowak et al., 2020) and plotted the angles as circular histograms (Fig. 6B). We analysed the perpendicularity (i.e. deviations from the cell growth axis of the filaments) and randomness (i.e. the degree of coherence of the filaments) of the resulting histograms (Fig. 6C,D). In agreement with our observations, both the actin and microtubule cytoskeletal arrays re-organized to align with the growth axis of the maturing cells (Fig. 6C). Whereas the actin array became increasingly more

Development (2022) 149, dev200415. doi:10.1242/dev.200415

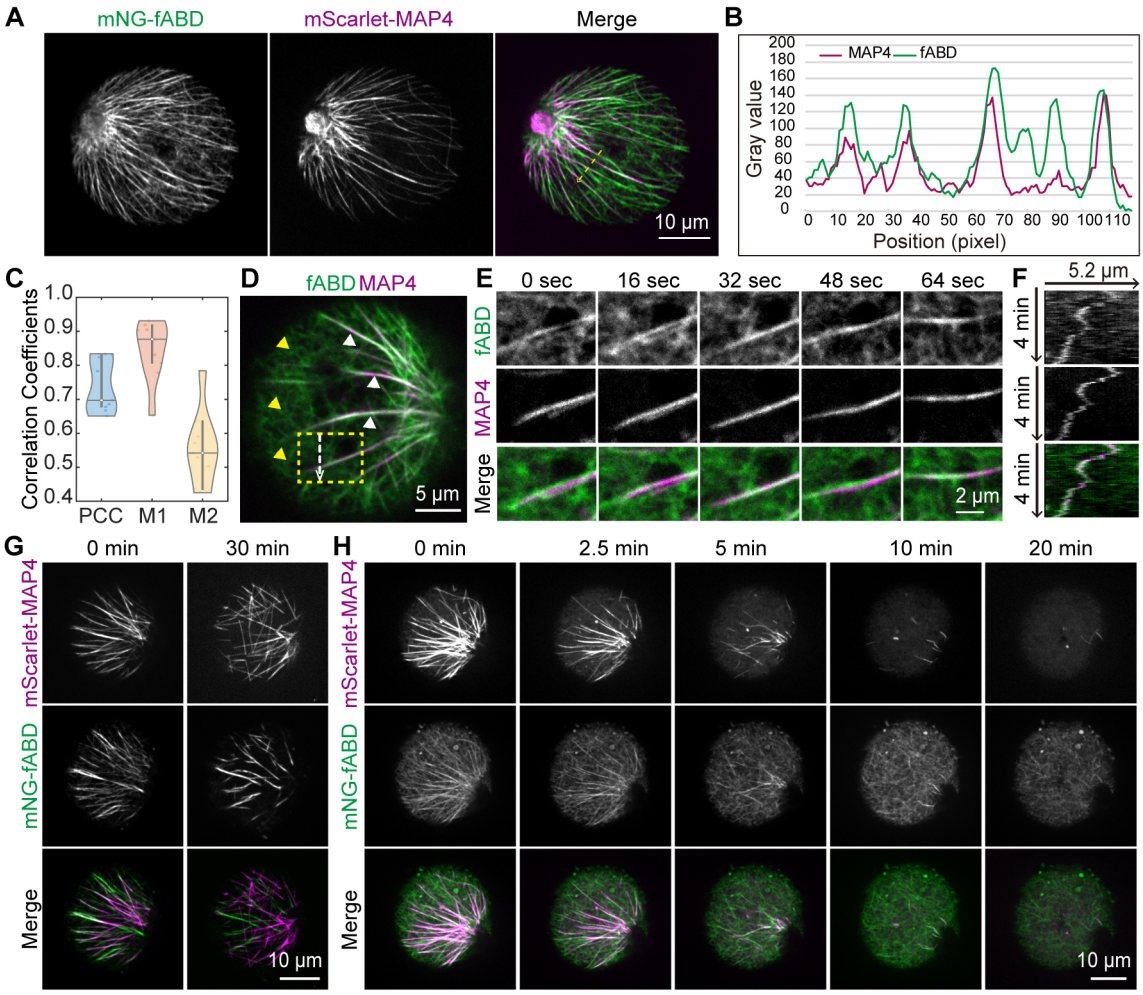

Fig. 4. The actin and microtubule cytoskeletons engage with each other during rice pollen development. (A) Colocalization between actin and microtubule cytoskeletons in maturing rice pollen. Images were taken from the microtubule and actin dual-labelled line *RUBQ::mScarlet-MAP4 RUBQ::mNG-fABD*. (B) Line plot of the position of the dashed line in A. (C) Correlation coefficients between filamentous actin and microtubule fluorescence in pollen. PCC, Pearson correlation coefficient. Mander's coefficient test was used for M1 (the fraction of mScarlet-MAP4 in mNG-fABD) and M2 (the fraction of mNG-fABD in mScarlet-MAP4). *n*=10 pollen grains. (D) Representative image of a rice pollen grain showing partial colocalization between filamentous actin and microtubules. The white arrowheads indicate actin bundles and yellow arrowheads indicate fine actin filaments, which show low colocalization with microtubules. (E) A time series showing association between actin bundles and microtubules as they migrate. The imaged region was from the yellow dashed line box in D, with a time interval of 4 s. (F) Kymographs showing the co-migration of the actin bundle (top) and microtubule (middle). The kymograph line is indicated by the white dashed line arrow in D. (G) Treatment of rice pollen with 1 μM latrunculin B (actin inhibitor). The decreased abundance of filamentous actin after the treatment indicates partial actin depolymerization. (H) Treatment of rice pollen with 1 μM oryzalin (microtubule inhibitor). Time interval was 0.5 min. The images in A, G and H are maximum projections; images in D and E are single focal frames.

directional in maturing root cells, the microtubule array re-oriented in a coordinated fashion where the array maintained high directionality during the re-arrangement (Fig. 6C,D). We also noted similar actin array re-organization in other maturing cell types, such as anther epidermis (Fig. S4). We speculate that the cytoskeletal array re-organization may be a common procedure during interphase cell maturation.

The actin cytoskeleton sustains microtubule re-emergence during salt stress in rice root cells

Apart from supporting plant development, the cytoskeleton also plays crucial roles in adapting to changes in environmental conditions. For example, the microtubule array is sensitive to salt (NaCl) treatment, which causes rapid depolymerization in Arabidopsis (Endler et al., 2015). To assess how salt impacts the cytoskeletons in rice, dual-labelled rice seedlings (5 days after the crown root emerged) were incubated in NaCl-containing (250 mM) liquid medium. As in Arabidopsis, microtubules rapidly de-polymerized and re-emerged over time (Fig. 7A, Table S2). The response period and extent correlated with seedling age and root cell type. The younger the seedling, the more rapidly it responded (Fig. S5). Microtubule adjustments, both de-polymerization and recovery, started from the root tip and progressively responded upwards along the root (Fig. S6). During microtubule de-polymerization, we observed apparent fluorescent foci. These were initially few and relatively small, but gradually grew larger with time until microtubules disappeared (Fig. 7A from 2 h to 4 h, Table 1). During microtubule recovery, the large foci seemed to form new microtubules and we only observed small foci that gradually disappeared (Fig. 7A from 6 h to 8 h, Table 1). At later time points, microtubule arrays recovered and almost no foci were observed (Fig. 7A 8 h, Table 1, Table S2). However, the microtubule density never reached the levels of those prior to treatment (Fig. 7A, control versus 8 h, Table S2), 77.1 microtubule

Development (2022) 149, dev200415. doi:10.1242/dev.200415

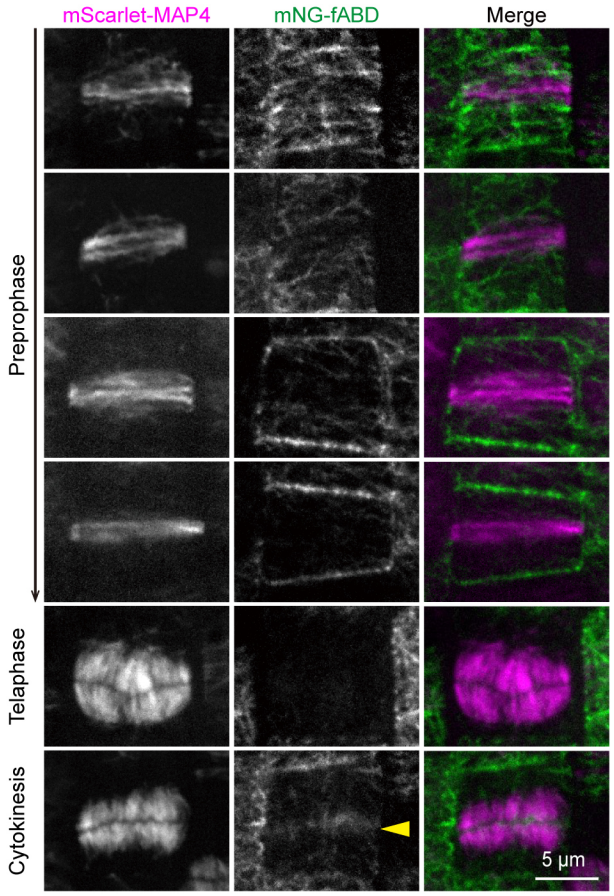

Fig. 5. Organization of filamentous actin and microtubules in dividing root cells of rice. The root tips of actin and microtubule dual-labelled rice lines were used for the observations. The images are all maximum projections. The filamentous actin signal changes during the preprophase band formation (top four images for mNG-fABD). Yellow arrowhead indicates fine actin filaments associating with the growing cell plate.

filaments per cell (counted from ten control cells) compared with 13.79 in cells treated by salt for 8 h, indicating that microtubule recovery was only partial. In contrast to the microtubule array, no major depolymerization events were observed for the actin cytoskeleton during the salt treatment. Indeed, actin filaments were abundant and maintained to a similar degree as those of the control cells (see mNG-fABD channel in Fig. 7A). Therefore, we conclude that the actin cytoskeleton is more tolerant to salt stress than microtubules.

These results prompted us to investigate whether the actin cytoskeleton has a function in sustaining the microtubule response during salt stress. To assess this further, we looked at both actin cytoskeleton and microtubule dynamics during salt treatment. During microtubule disassembly, small microtubule-related fluorescent foci formed and subsequently began to merge to form larger foci (Fig. 7B). Interestingly, these events coincided with actin filaments (Fig. 7B, Movie 6). Moreover, simultaneous treatment with NaCl and the actin disruptor latrunculin B delayed the formation of larger microtubule-related foci (Fig. 7C). Furthermore, separating microtubule-related foci associated with, and tracked along, actin filaments (Fig. 7D, Movie 7). Again, the disruption of the actin filaments caused a substantial delay in microtubule recovery (Fig. 7E). We therefore propose that actin filaments facilitate rapid re-emergence of microtubules during salt exposure.

RMD supports actin bundling in rice coleoptile cells

Rice morphology determinant (RMD) encodes the rice formin 5 protein, which binds to and bundles actin filaments (Zhang et al., 2011). RMD controls many aspects of rice biological processes, including light responses (Fig. 8A; Song et al., 2019). These results make *rmd-1* an ideal genotype to assess the actin array organization and behaviour using our actin fluorescent markers. We therefore crossed the *rmd-1* mutant lines with the *mNG-fABD*-expressing line. We next investigated the actin array in 5-day-old dark- and light-grown *rmd-1* coleoptiles. We found that the actin cytoskeletal organization in the *rmd-1* mutant was different from that in wild type (Fig. 8B). Detailed inspection of the actin organization revealed less actin bundling in the *rmd-1* mutant than in wild type. To quantify any differences in the actin array organization, we again employed Cytoseg2.0 (Nowak et al., 2020). Using this algorithm, we confirmed the reduced actin bundling in the *rmd-1* mutant (Fig. 8C). In addition, quantitative analyses revealed that the actin filaments were less coherent in the *rmd-1* mutant than in wild type (Fig. 8D) and consequently aligned less well with the major cell axis (Fig. 8E). Interestingly, the actin bundling was significantly reduced in light-grown seedlings compared with dark-grown seedlings (Fig. 8B,C, Table S3), perhaps reflecting a role of actin bundles in rapid cell expansion. Interestingly, this scenario was reversed in the *rmd-1* mutant (Fig. 8B,C, Table S3). We also observed the microtubule array in the *rmd-1* mutant. Compared with wild type, the *rmd-1* mutant displayed some disturbance in the microtubule array, notably in light-germinated coleoptiles (Fig. S7). However, the differences were less pronounced than those observed for the actin cytoskeleton. These differences might explain why the *rmd-1* mutant displays a shoot-bending phenotype in light (Fig. 8A).

DISCUSSION

We established bright and stable fluorescent cytoskeleton markers in rice to facilitate live-cell imaging of the actin and microtubule cytoskeletons (Figs 1, 2). We found that both *Ubi1* and *RUBQ2* promoters can be used to drive fABD and MAP4 to get homogeneous, bright and stable actin and microtubule fluorescence. For microtubule labelling, we advise using the *Ubi1* promoter because the high expression of the *RUBQ2* promoter tends to cause abnormal plant phenotypes (Fig. S1). Although the 35S promoter appears to induce silencing in many rice tissues, it generated good fluorescent signals in stomata (Fig. 1) and could be useful for stomata functional studies. In contrast to Arabidopsis, the use of rice tubulin subunits did not label microtubules well *in planta* (Fig. 1B) and caused phenotypic deviations from wild type. Other proteins, such as Lifeact, mTalin and KMD, etc. (Kost et al., 1998; Vidali et al., 2009; Deeks et al., 2010), can also be tested as potential rice cytoskeleton-labelling strategies.

Although we observed cytoskeletal fluorescence in developing pollen, we did not observe any signals in pollen mother cells (Fig. S2). It is plausible that this is because the cytoskeleton is too diffuse to be observed reliably with our markers. In future studies, it could be worthwhile to test meiosis-specific promoters to drive fABD/MAP4 to study early rice pollen development, because many rice male sterile-related events are determined at the early microspore stages (Wang et al., 2017; Zhang et al., 2019). Currently, cytoskeleton studies in pollen are mainly focused on pollen germination and pollen tube growth (Chang and Huang, 2015; Liu et al., 2018). By contrast, cytoskeletal function and organization are understudied during pollen grain development. Here, we recorded this process and found that both actin filaments and

Development (2022) 149, dev200415. doi:10.1242/dev.200415

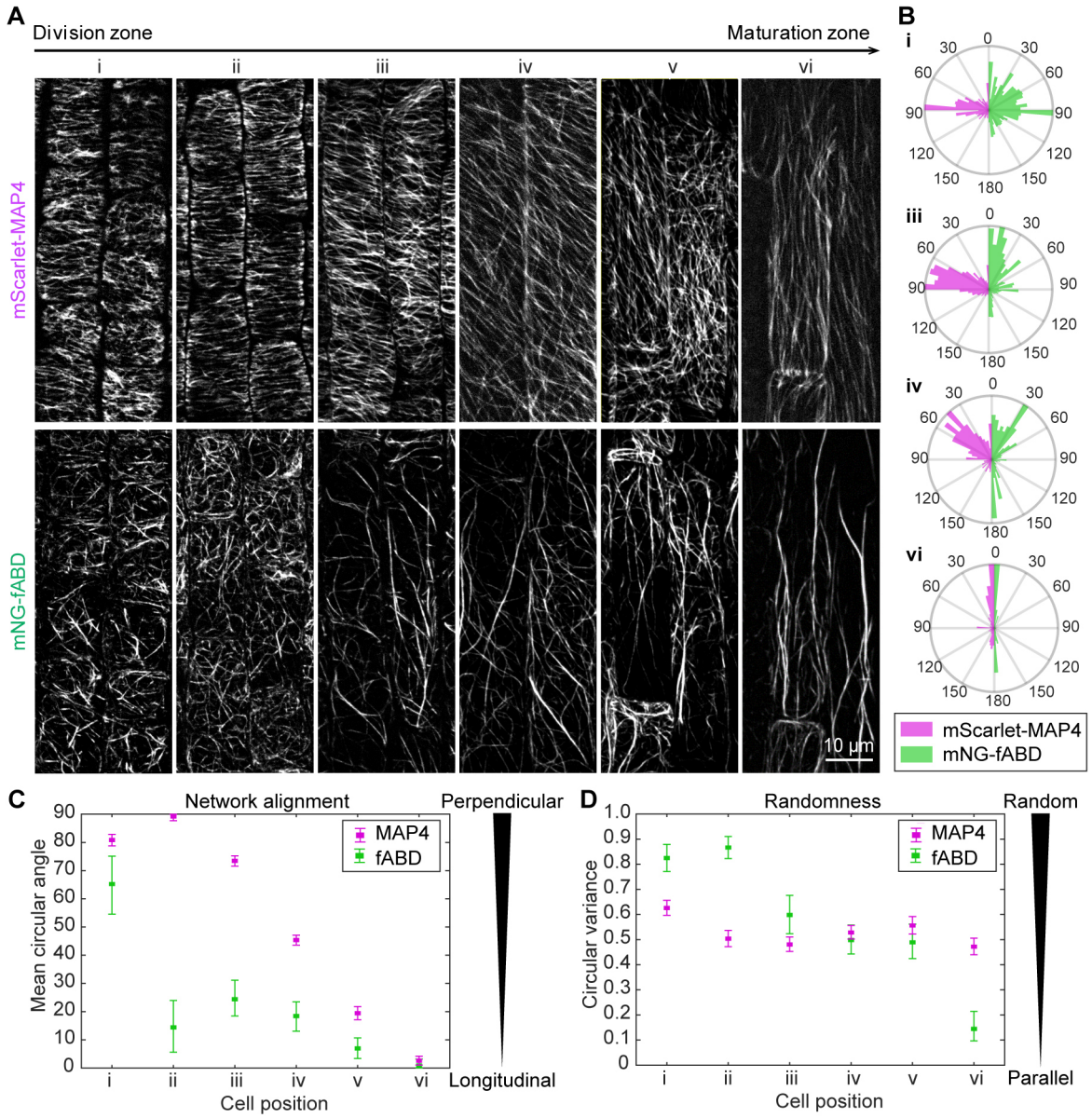

Fig. 6. The actin and microtubule cytoskeletons re-orient in a coordinated fashion during cell growth in rice root. (A) Images tracking cytoskeleton redirection during root cell growth. The images from left to right were taken from the root tip region to the maturing region in the dual-labelled line. The images are maximum projections from *z*-stacks of root epidermal cells. (B) Circular histograms for all edge angles (weighted by edge length) of the actin and microtubule cytoskeletons, extracted from selected images in A using Cytoseg2.0. The major axis of the cell (longitudinal) is defined as 0°. (C) Quantification of changes in the network alignment for filamentous actin and microtubules from the images in A. Large angles describe a network that is oriented perpendicular to the major cell axis; small angles indicate longitudinal orientation. (D) Quantification of network randomness for filamentous actin and microtubules from the images in A. Small values describe a network with parallel edges; large values indicate a wider distribution of edge orientation.

microtubules change from a disordered to ordered organization (Fig. 3). We note that previous studies did not report the highly ordered/radial microtubule structure that we observed (Zee and Ye, 2000). It is worth noting that this study used immunolabelling to visualize the microtubules. It is therefore possible that certain developmental stages were missed or that the fixation and staining process damaged the microtubule structure, as we found it to be sensitive to stresses (Fig. 4G, Fig. S3). Such differences highlight the advantages of live-cell imaging that more accurately capture the 'natural' state of the cytoskeleton.

The interplay between the actin and microtubule cytoskeleton has been a longstanding research topic in animal cells (Dogterom and Koenderink, 2019). In plant cells, scientists have speculated that the two cytoskeletal polymers interact to fulfil cellular activities (Petrášek and Schwarzerová, 2009). Indeed, several proteins have the ability to associate with both actin and microtubules (Zhang et al., 2011; Sun et al., 2017). In addition, repolymerization of actin filaments occurred along microtubules in Arabidopsis cells (Sampathkumar et al., 2011). The tight co-alignment of actin bundles and microtubules in maturing rice pollen that we observed (Fig. 4A-E) adds to our understanding of these connections. Here, we found that actin filaments are necessary to maintain radial microtubule distribution and that microtubules are essential for actin bundle formation (Fig. 4F,G). However, the proteins that facilitate these interactions and the biological function of the radial patterns remain to be addressed.

Development (2022) 149, dev200415. doi:10.1242/dev.200415

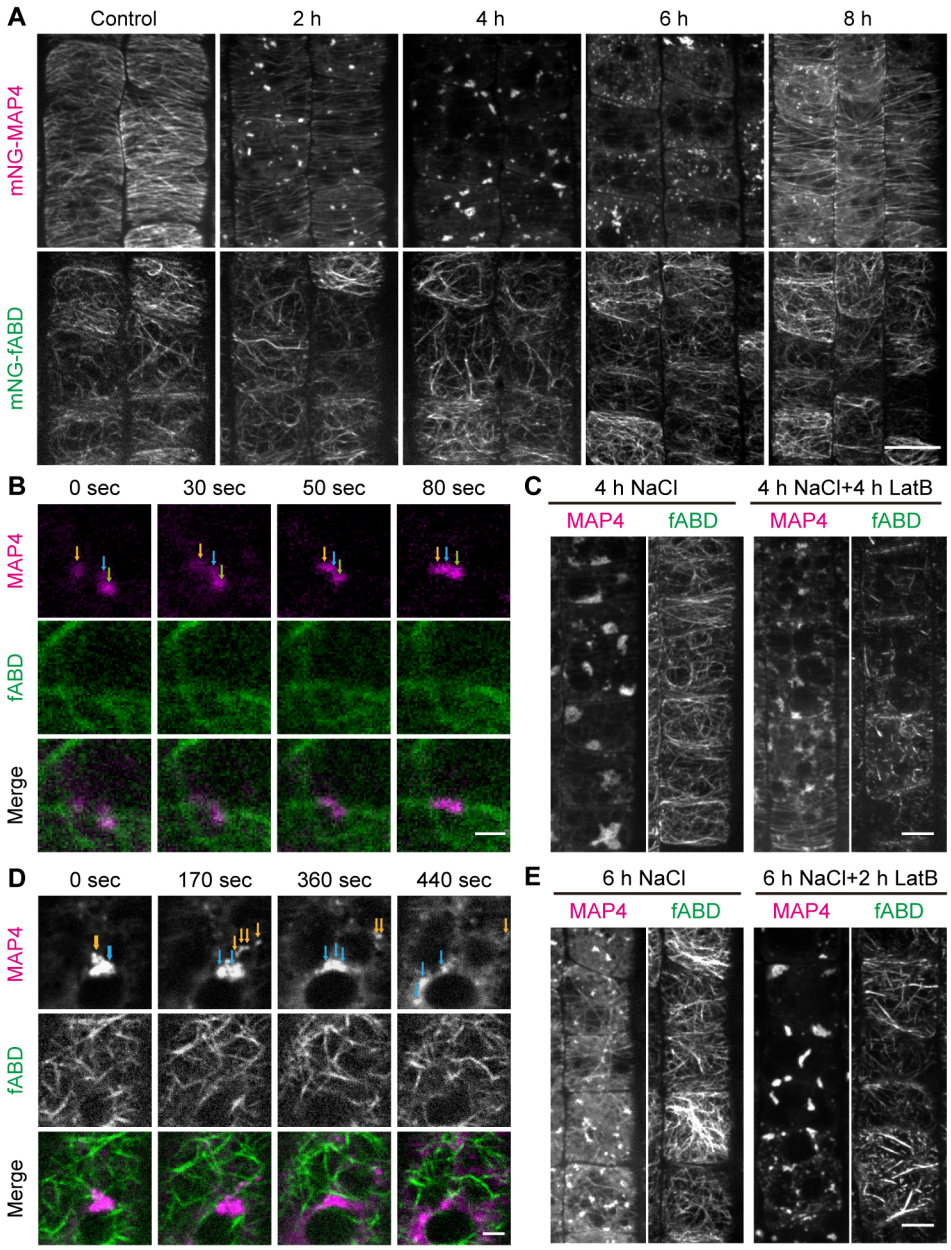

Fig. 7. The actin cytoskeleton facilitates microtubule re-emergence upon salt treatment. (A) Actin (mNG-fABD) and microtubule (mScarlet-MAP4) cytoskeleton response to salt treatment. Five-day-old seedlings (after crown root emergence) were incubated with 250 mM NaCl-containing liquid medium for the indicated time. The epidermal cells of dual-labelled lines were imaged by *z*-scanning. The images of the root transition zone (see schematic definition in Fig. S6) are maximum projections and cropped. Scale bar: 10 µm. (B) Time-lapse series to show the merge of microtubule-related foci. Seedlings were incubated with salt for 1.5 h. The arrows are tracking the positions of microtubule-related foci. Scale bar: 1 µm. (C) Microtubule-related foci formation after 4 h salt incubation with or without 0.5 µM latrunculin B (LatB). Scale bar: 5 µm. (D) Time-lapse series to show the separation of microtubule-related foci. Seedlings were incubated with salt for 5 h. The arrows are tracking the separation of microtubule-related foci. Scale bar: 2 µm. (E) Microtubule-related foci disappearance after 6 h salt incubation with or without LatB. LatB was added at 4 h after salt incubation. Scale bar: 5 µm. Images in C and E are maximum projections.

Soil salinization is a severe agricultural problem in crop production (Mukhopadhyay et al., 2021). Microtubules play an important role in the plant salt tolerance (Chun et al., 2021), and the response of the microtubules to salt has been well documented in Arabidopsis (Wang et al., 2007; Endler et al., 2015). We report a similar response of microtubules during salt stress in rice roots, including depolymerization and subsequent reassembly (Fig. 7A, Table S2). However, we also observed that the re-assembly of microtubules appear to be generated via microtubule-related foci (Fig. 7A, Table 1). We speculate that these foci may act as temporary microtubule ‘reserves’ to recover the microtubule array. Consistent with this, the foci appeared to be guided by the actin cytoskeleton (Fig. 7B,D), a notion supported by actin cytoskeleton depolymerization, which caused significant delay in microtubule recovery (Fig. 7C,E). This emphasizes an important function of the actin cytoskeleton during salt stress. The intact actin cytoskeleton may also be important to maintain cell activity, such as trafficking, during salt exposure. To sum up, by using live-cell imaging of actin and microtubule dual-labelled lines, combined with drug treatment, we found that actin filaments support the formation and separation of microtubule-related foci during salt exposure (Fig. 7B-E), and are important for microtubule recovery. Consistently, several actin-associated proteins positively regulate

Table 1. Quantification of microtubule foci after salt treatment

Time point	Median radius (pixels)	Median absolute deviation	Number of cells	Mean number per cell
1.5-2 h	4.07	0.68	96	4.80
3.5-4 h	4.99	1.26	111	8.62
5.5-6 h	2.93	0.89	122	7.35
7.5-8 h	3.64	0.57	138	1.03

The seedlings were incubated with 250 mM NaCl for the indicated times. Microtubule-related foci size (radius in pixels) and number were analysed by Laplace of Gaussian method. The root transition zones of five seedlings were used for analysis at each time point (see Fig. 7 for other details).

Development (2022) 149, dev200415. doi:10.1242/dev.200415

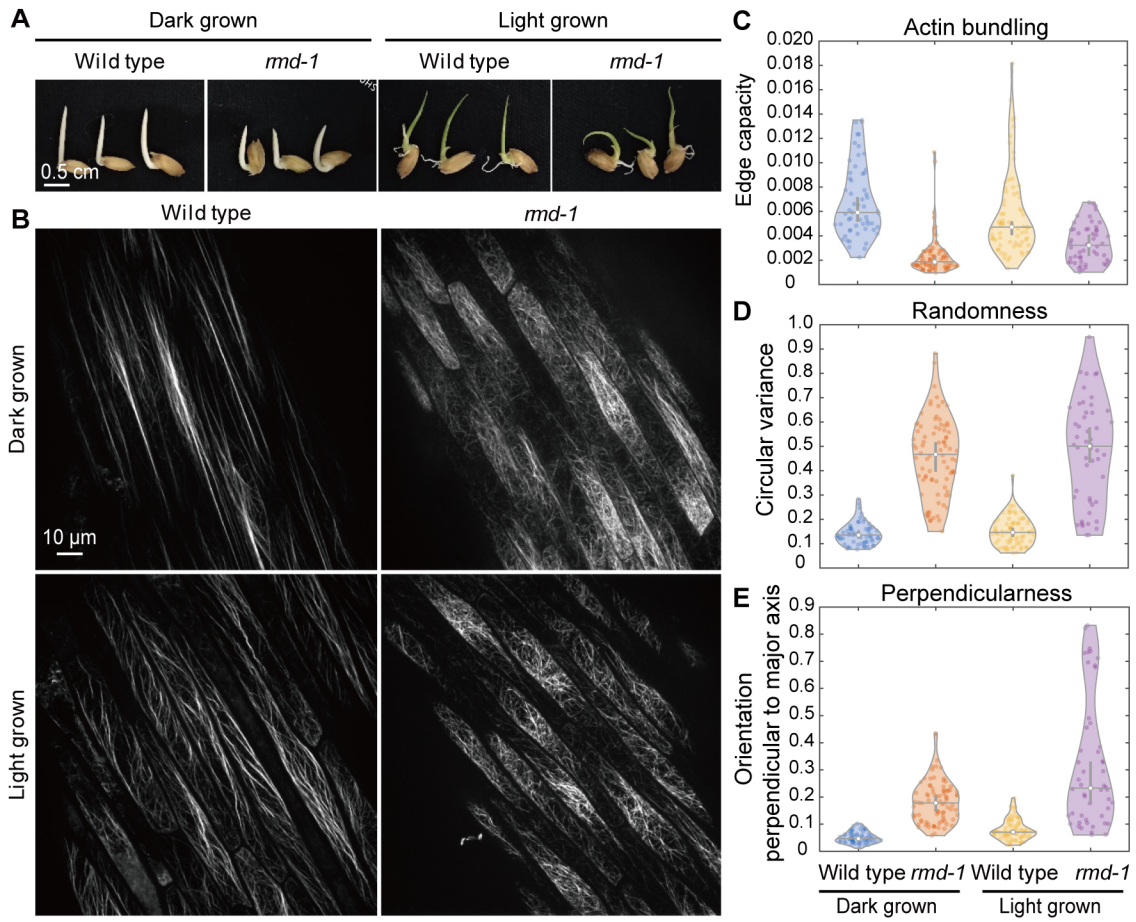

Fig. 8. Live-cell imaging reveals that RMD supports actin bundling in rice interphase cells. (A) Rice seedlings (wild type and *rmd-1* mutant) were germinated in light and dark for 5 days. The crown roots were removed. (B) Maximum-projection images of actin cytoskeleton in the epidermis of coleoptiles germinated for 4 days. Note the filamentous actin pattern and distribution in the cells. (C) Quantification of actin bundling in dark-grown coleoptiles (*n*=57 cells for wild type and *n*=84 cells for *rmd-1*) and in the light (*n*=71 cells for wild type and *n*=50 cells for *rmd-1*) of wild type and *rmd-1* mutants using Cytoseg2.0. (D) Quantification of the network randomness for the cells analysed in C (for more details on the circular statistics see Fig. S8). (E) Quantification of the network perpendicularity for the cells analysed in C.

salt tolerance (Zhao et al., 2013; Sengupta et al., 2019; Wang et al., 2021).

Taken together, we generated rice cytoskeleton fluorescent markers and convincingly show that live-cell imaging of the cytoskeletal components in rice can provide new insights into the function of some of the most important polymers in plant cell biology and development.

MATERIALS AND METHODS

Plasmid constructs

All plasmids generated for this publication are based on the vector pCAMBIA1301 (GenBank accession number AF234297.1). For the 35S-driven plasmid, the *GFP* was inserted at the *Nco*I site and the *fABD*/*MAP4* was inserted between the *Bgl*II and *BstE*II sites. For the *Ubi1*-driven GFP lines, *Ubi1* and *GFP* were inserted at the *EcoR*I and *Kpn*I site, respectively; the *OsfABD*/*OsTUA1* was inserted between the *Hind*III and *Pml*I sites. For other plasmids, the promoters *Ubi1* or *RUBQ* were inserted at the *EcoR*I site; the fluorescent protein-coding sequences *mNeonGreen* or *mScarlet* were inserted between the *Kpn*I and *BamH*I sites; and the *fABD*/*MAP4* was inserted between the *BamH*I and *BstE*II sites.

The promoters *Ubi* and *RUBQ* were amplified from the vectors pTCK303 (Wang et al., 2004) and pRGEB3.2 (Xie et al., 2015). The licenses for using fluorescent proteins mNeonGreen and mScarlet were purchased from Allele Biotechnology and Pharmaceuticals (San Diego, CA, USA) (Shaner et al., 2013; Bindels et al., 2017). The *AtfABD* and *MAP4* were amplified from the Arabidopsis seedlings of *35S::GFP-fABD* (Sheahan et al., 2004) and *35S::mCherry-MAP4* (Gutierrez et al., 2009), respectively. The *OsfABD* (LOC_Os02g48740) and *OsTUA1* (LOC_Os03g51600) were amplified from rice cDNA. All amplification primers are included in Table S4.

The plasmids were transformed into rice calli (*Oryza sativa* Japonica, cultivar 9522) by agroinfiltration. Transgenic plants were obtained through the skilled technology in our laboratory as reported previously (Cao et al., 2020).

Plant growth conditions

To germinate the seeds, glass Petri dishes were used with a layer of filter paper placed at the bottom. No more than 50 seeds were put on the paper, and deionized water was added until the seeds were just covered. The Petri dish was then put into a Percival (E-36L2, Percival Scientific, Perry, IA, USA) growth chamber (condition: 16 h light/8 h dark and 28°C/23°C) for germination. Aluminium foil was used to cover the Petri dish to induce etiolated coleoptiles. After 4 days of germination, the seeds were used for coleoptile imaging. After germinating for 5 days, the seedlings were transferred into liquid 1/2 Murashige and Skoog (MS) medium for further growth in a black box with a black cover. The cover had small holes to hold the seedlings, letting roots grow into the liquid. These roots were used for imaging. To get adult plants, the rice seedlings were grown in the growth chamber for ∼1 month and then transferred to soil. In the summer, the adult rice plants were grown in the field; in the winter, they were grown in a greenhouse until flowering and seed setting.

Development (2022) 149, dev200415. doi:10.1242/dev.200415

Sample preparation

For normal imaging, the tissues were usually detached from the entire seedling/plant and the epidermis was imaged. Young stem at tillering stage was sliced into 0.5 cm^2 pieces of 1 mm thickness. The epidermis (~0.5 cm^2) was taken by tweezers from the coleoptile, and the leaf was grown in less than 10 days. Then, 0.5-1 cm length root tips were imaged at the indicated age in each particular experiment. Anthers were removed from spikelets and directly mounted without any process. Pollen was prepared for imaging as described in the Pollen imaging section.

A 3 mm-thick special metal holder slide, with a round hole (diameter 1.5 cm) in the middle, was used to mount the samples. During imaging, the samples were placed in the hole held by a cover slide stuck on one side of the metal slide. A prepared round agar pad was used to cover the samples.

Pollen imaging

To image pollen, the preparation was slightly modified from those for normal sample imaging. One drop of water (~20 µl) was kept at the hole place on the cover slide stuck on the bottom side of the metal slide. Anthers from one spikelet were taken into the water and then the anthers were repeatedly squeezed using a tweezer, releasing pollen into the water. The anther residue was removed. Then, another cover slide was stuck on the top of the metal slide without directly touching the pollen samples, making a free space in between and protecting against water evaporation.

For the drug treatment, the water contained 1 µM oryzalin (19044-88-3, Sigma-Aldrich) or latrunculin B (76343-94-7, Sigma-Aldrich). Once the pollen was released into the drug-containing water, the treatment started and the imaging began immediately.

To germinate pollen, the shedding pollen was scattered on the solid pollen germination medium (Liu et al., 2018). To image hydrated pollen, a small piece of medium containing the pollen was directed taken on the prepared slide for imaging after 5 min. To get pollen tubes, the pollen was incubated in the medium for 1 h at 37°C.

Salt treatment and imaging preparation

For the NaCl treatment, rice seedlings grown in a black box for 4-5 days were used. The root parts of the seedlings were incubated (80 rpm shaking) in liquid 1/2 MS medium containing 250 mM NaCl (CAS:7647-14-5, Sinoreagent, Shanghai, China). After the indicated incubation times, 0.5-1 cm (from the root tip) roots were detached from the seedlings and mounted on slides with the NaCl-containing medium. The epidermises of roots were imaged.

Live-cell imaging

Unless specified otherwise, images in this article were taken with a spinning disk confocal microscope (SpinSR, Olympus, Tokyo, Japan) equipped with a CSU-W1 disk (Yokogawa, Tokyo, Japan). Both 100× (1.50 NA, oil) and 60× (1.35 NA, silicone oil) objectives were used in an Olympus inverted imaging platform IX83 System. Lasers of 488 nm and 561 nm were used to excite the mNeongreen/GFP and mScarlet proteins, and the emission filters were bandpass 525/50 and 617/73, respectively. Unless specified otherwise, *z*-stacks were acquired with a step size of 0.5 µm. The time intervals of time series are indicated in the figure legends.

Image processing and analysis

All images shown in this paper were preprocessed in Fiji (Schindelin et al., 2012), which usually included contrast adjustment, background subtraction and maximum projection (unless indicated otherwise). Image analysis was done using unprocessed maximum projections of the acquired *z*-stacks. Colocalization tests were done using the Fiji plugin JACoP (Bolte and Cordelières, 2006), in which Mander's coefficient and Pearson correlation coefficient analyses were performed. The microtubule-related foci were analysed using the Python package of skimage.feature.blob_log (van der Walt et al., 2014). The microtubule filament number after salt treatment was analysed using a custom-built script developed in Python 3.8.

Quantification of the cytoskeletal organization for both actin and microtubule marker lines was performed using Cytoseg2 (Nowak et al., 2020). The algorithm uses graph theory to describe and create a connected graph of the organization of the filaments. From the connected undirected graph, all edges of the networks were extracted and analysed in MATLAB (MathWorks, Natick, MA, USA) using four parameters: (1) the filament bundling in the network, given by the edge capacity (edge intensity normalized by length); (2) the network alignment with respect to the major cell axis, given by the weighted mean circular angle (Fisher, 1993; Jammalamadaka and SenGupta, 2001; Berens, 2009); (3) the randomness of the network, given by the weighted circular variance (Berens, 2009); and (4) the perpendicularity of the network, given by the weighted median of all smallest angles between each edge and the major cell axis. For all angle parameters (2-4), the edge angles were weighted by the total intensity of each edge.

The extracted data were analysed by circular statistics (see Fig. S8). Because some networks can show a bimodal distribution (4 in Fig. S8), all angles were multiplied by 2, before estimating the mean circular angle and dividing the result by 2 (angle doubling; Fisher, 1993). Estimating the correct mean circular angle from these simulated networks only works for directed networks (3-5 in Fig. S8). Very random networks (1-2 in Fig. S8) look very similar and because the angle distribution is very uniform, the mean circular angle is not a useful parameter for these networks. Therefore, we introduced the perpendicularity parameter. Here, the smallest angle between each edge and the major cell axis is calculated, restricting all angles to 0-90°. Then, the weighted median of these angles is estimated. In order to avoid confusion with the mean circular angle, the resulting weighted median is rescaled from 0-90° to 0-1. For random networks, the perpendicularity will be ≈0.5 (1-2 in Fig. S8); for directed networks with a 45° angle, the perpendicularity is also ≈0.5 (3 in Fig. S8), but for longitudinal oriented networks the value is close to 0 (4 in Fig. S8) and for perpendicular oriented networks it is close to 1 (5 in Fig. S8).

Acknowledgements

We thank the Core Facility and Technical Service Center, School of Life Science and Biotechnologies [Shanghai Jiao Tong University (SJTU), Shanghai, China] for assistance with confocal microscopy, and Mingjiao Chen (SJTU) and Xiaofei Chen (SJTU) for the rice callus transformation and transgenic plant selection.

Competing interests

The authors declare no competing or financial interests.

Author contributions

Conceptualization: Z.L., W.C., S.P., D.Z.; Methodology: Z.L., I.Ø., F.R.; Validation: Z.L.; Investigation: Z.L., I.Ø., F.R., Y.C., G.H., W.C., J.Z.; Resources: Z.L., D.Z.; Data curation: Z.L., I.Ø., F.R.; Writing - original draft: Z.L.; Writing - review & editing: Z.L., I.Ø., F.R., W.C., J.Z., W.L., Z.N., S.P., D.Z.; Visualization: Z.L.; Supervision: W.L., Z.N., S.P., D.Z.

Funding

This work was funded by the National Natural Science Foundation of China (31970803, 32130006 and 31701166), the National Natural Science Foundation of China and the Deutsche Forschungsgemeinschaft (China-Germany Mobility Program, M-0141), Shanghai Jiao Tong University (Startup Fund for Young Researcher, AF0800067; Joint International Research Laboratory of Metabolic and Developmental Sciences Joint Research Fund, MDS-JF-2019A05), China Postdoctoral Science Foundation (2017M621451), Ministry of Education of the People's Republic of China (111 Project, B14016), Syddansk Universitet VILLUM Center for Bioanalytical Sciences (25915), Novo Nordisk Fonden (19OC0056076), Danmarks Grundforskningsfond (DNRF155) and Australian Research Council Discovery Project (DP190101941 and DP210100956).

References

Adamowski, M., Li, L. and Friml, J. (2019). Reorientation of cortical microtubule arrays in the hypocotyl of *Arabidopsis thaliana* is induced by the cell growth process and independent of auxin signaling. *Int. J. Mol. Sci.* **20**, 3337. doi:10.3390/ijms20133337

Berens, P. (2009). CircStat: a MATLAB toolbox for circular statistics. *J. Stat. Softw.* **1**, 1-21. doi:10.18637/jss.v031.i10

Bindels, D. S., Haarbosch, L., van Weeren, L., Postma, M., Wiese, K. E., Mastop, M., Aumonier, S., Gotthard, G., Royant, A., Hink, M. A Jr. et al. (2017). mScarlet: a bright monomeric red fluorescent protein for cellular imaging. *Nat. Methods* **14**, 53-56. doi:10.1038/nmeth.4074

Bolte, S. and Cordelières, F. P. (2006). A guided tour into subcellular colocalization analysis in light microscopy. *J. Microsc.* **224**, 213-232. doi:10.1111/j.1365-2818.2006.01706.x

Cao, Y., Cai, W., Chen, X., Chen, M., Chu, J., Liang, W., Persson, S., Liu, Z. and Zhang, D. (2020). Bright fluorescent vacuolar marker lines allow vacuolar tracing across multiple tissues and stress conditions in rice. *Int. J. Mol. Sci.* **21**, 4203. doi:10.3390/ijms21124203
Chan, J. (2012). Microtubule and cellulose microfibril orientation during plant cell and organ growth. *J. Microsc.* **247**, 23-32. doi:10.1111/j.1365-2818.2011.03585.x
Chang, M. and Huang, S. (2015). Arabidopsis ACT11 modifies actin turnover to promote pollen germination and maintain the normal rate of tube growth. *Plant J.* **83**, 515-527. doi:10.1111/tpj.12910
Chang, S., Ren, Z., Liu, C., Du, P., Li, J., Liu, Z., Zhang, F., Hou, H., Shi, J., Liang, W. et al. (2021). *OsFH3* encodes a type II formin required for rice morphogenesis. *Int. J. Mol. Sci.* **22**, 13250. doi:10.3390/ijms222413250
Chun, H. J., Baek, D., Jin, B. J., Cho, H. M., Park, M. S., Lee, S. H., Lim, L. H., Cha, Y. J., Bae, D. W., Kim, S. T. et al. (2021). Microtubule dynamics plays a vital role in plant adaptation and tolerance to salt stress. *Int. J. Mol. Sci.* **22**, 5957. doi:10.3390/ijms22115957
Courtemanche, N., Pollard, T. D. and Chen, Q. (2016). Avoiding artefacts when counting polymerized actin in live cells with LifeAct fused to fluorescent proteins. *Nat. Cell Biol.* **18**, 676-683. doi:10.1038/ncb3351
Deeks, M., Fendrych, M., Smertenko, A., Bell, K., Oparka, K., Cvrčková, F., Žárský, V. and Hussey, P. (2010). The plant formin AtFH4 interacts with both actin and microtubules, and contains a newly identified microtubule-binding domain. *J. Cell Sci.* **123**, 1209-1215. doi:10.1242/jcs.065557
Dogterom, M. and Koenderink, G. H. (2019). Actin-microtubule crosstalk in cell biology. *Nat. Rev. Mol. Cell Biol.* **20**, 38-54. doi:10.1038/s41580-018-0067-1
Endler, A., Kesten, C., Schneider, R., Zhang, Y., Ivakov, A., Froehlich, A., Funke, N. and Persson, S. (2015). A mechanism for sustained cellulose synthesis during salt stress. *Cell* **162**, 1353-1364. doi:10.1016/j.cell.2015.08.028
Fisher, N. I. (1993). *Statistical Analysis of Circular Data*. Cambridge: Cambridge University Press.
Flores, L. R., Keeling, M. C., Zhang, X., Sliogeryte, K. and Gavara, N. (2019). Lifeact-TagGFP2 alters F-actin organization, cellular morphology and biophysical behaviour. *Sci. Rep.* **9**, 3241. doi:10.1038/s41598-019-40092-w
Gutierrez, R., Lindeboom, J. J., Paredez, A. R., Emons, A. M. and Ehrhardt, D. W. (2009). Arabidopsis cortical microtubules position cellulose synthase delivery to the plasma membrane and interact with cellulose synthase trafficking compartments. *Nat. Cell Biol.* **11**, 797-806. doi:10.1038/ncb1886
Huang, G., Liang, W., Sturrock, C. J., Pandey, B. K., Giri, J., Mairhofer, S., Wang, D., Muller, L., Tan, H., York, L. M. et al. (2018). Rice actin binding protein RMD controls crown root angle in response to external phosphate. *Nat. Commun.* **9**, 2346. doi:10.1038/s41467-018-04710-x
Jammalamadaka, S. R. and SenGupta, A. (2001). *Topics in Circular Statistics*, Vol. 5. World Scientific.
Komorisono, M., Ueguchi-Tanaka, M., Aichi, I., Hasegawa, Y., Ashikari, M., Kitano, H., Matsuoka, M. and Sazuka, T. (2005). Analysis of the rice mutant dwarf and gladius leaf 1. Aberrant katanin-mediated microtubule organization causes up-regulation of gibberellin biosynthetic genes independently of gibberellin signaling. *Plant Physiol.* **138**, 1982-1993. doi:10.1104/pp.105.062968
Kost, B., Spielhofer, P. and Chua, N. H. (1998). A GFP-mouse talin fusion protein labels plant actin filaments in vivo and visualizes the actin cytoskeleton in growing pollen tubes. *Plant J.* **16**, 393-401. doi:10.1046/j.1365-313x.1998.00304.x
Kost, B., Mathur, J. and Chua, N. H. (1999). Cytoskeleton in plant development. *Curr. Opin. Plant Biol.* **2**, 462-470. doi:10.1016/S1369-5266(99)00024-2
Li, G., Liang, W., Zhang, X., Ren, H., Hu, J., Bennett, M. J. and Zhang, D. (2014). Rice actin-binding protein RMD is a key link in the auxin-actin regulatory loop that controls cell growth. *Proc. Natl. Acad. Sci. USA* **111**, 10377-10382. doi:10.1073/pnas.1401680111
Lipka, E., Herrmann, A. and Mueller, S. (2015). Mechanisms of plant cell division. *Wiley Interdiscip. Rev. Dev. Biol.* **4**, 391-405. doi:10.1002/wdev.186
Liu, C., Zhang, Y. and Ren, H. (2018). Actin polymerization mediated by AtFH5 directs the polarity establishment and vesicle trafficking for pollen germination in arabidopsis. *Mol. Plant* **11**, 1389-1399. doi:10.1016/j.molp.2018.09.004
Lo, S.-F., Cheng, M.-L., Hsing, Y.-C., Chen, Y.-S., Lee, K.-W., Hong, Y.-F., Hsiao, Y., Hsiao, A.-S., Chen, P.-J., Wong, L.-I. et al. (2020). Rice big grain 1 promotes cell division to enhance organ development, stress tolerance and grain yield. *Plant Biotechnol. J.* **18**, 1969-1983. doi:10.1111/pbi.13357
Maeda, K. and Higaki, T. (2021). Disruption of actin filaments delays accumulation of cell plate membranes after chromosome separation. *Plant Signal Behav.* **16**, 1873586. doi:10.1080/15592324.2021.1873586
Maeda, K., Sasabe, M., Hanamata, S., Machida, Y., Hasezawa, S. and Higaki, T. (2020). Actin filament disruption alters phragmoplast microtubule dynamics during the initial phase of plant cytokinesis. *Plant Cell Physiol.* **61**, 445-456. doi:10.1093/pcp/pcaa003
Marc, J., Granger, C. L., Brincat, J., Fisher, D. D., Kao, T., McCubbin, A. G. and Cyr, R. J. (1998). A GFP-MAP4 reporter gene for visualizing cortical microtubule rearrangements in living epidermal cells. *Plant Cell* **10**, 1927-1940. doi:10.2307/3870914
Mohanty, A., Luo, A., DeBlasio, S., Ling, X., Yang, Y., Tuthill, D. E., Williams, K. E., Hill, D., Zadrozny, T., Chan, A. et al. (2009). Advancing cell biology and functional genomics in maize using fluorescent protein-tagged lines. *Plant Physiol.* **149**, 601-605. doi:10.1104/pp.108.130146
Mukhopadhyay, R., Sarkar, B., Jat, H. S., Sharma, P. C. and Bolan, N. S. (2021). Soil salinity under climate change: challenges for sustainable agriculture and food security. *J. Environ. Manage.* **280**, 111736. doi:10.1016/j.jenvman.2020.111736
Nowak, J., Gennermann, K., Persson, S. and Nikoloski, Z. (2020). CytoSeg 2.0: automated extraction of actin filaments. *Bioinformatics* **36**, 2950-2951. doi:10.1093/bioinformatics/btaa035
Panteris, E. (2008). Cortical actin filaments at the division site of mitotic plant cells: a reconsideration of the 'actin-depleted zone'. *New Phytol.* **179**, 334-341. doi:10.1111/j.1469-8137.2008.02474.x
Petrášek, J. and Schwarzerová, K. (2009). Actin and microtubule cytoskeleton interactions. *Curr. Opin. Plant Biol.* **12**, 728-734. doi:10.1016/j.pbi.2009.09.010
Qu, X., Zhang, R., Zhang, M., Diao, M., Xue, Y. and Huang, S. (2017). Organizational innovation of apical actin filaments drives rapid pollen tube growth and turning. *Mol. Plant.* **10**, 930-947. doi:10.1016/j.molp.2017.05.002
Sampathkumar, A., Lindeboom, J. J., Debolt, S., Gutierrez, R., Ehrhardt, D. W., Ketelaar, T. and Persson, S. (2011). Live cell imaging reveals structural associations between the actin and microtubule cytoskeleton in Arabidopsis. *Plant Cell* **23**, 2302-2313. doi:10.1105/tpc.111.087940
Schindelin, J., Arganda-Carreras, I., Frise, E., Kaynig, V., Longair, M., Pietzsch, T., Preibisch, S., Rueden, C., Saalfeld, S., Schmid, B. et al. (2012). Fiji: an open-source platform for biological-image analysis. *Nat. Methods* **9**, 676-682. doi:10.1038/nmeth.2019
Seck, P. A., Diagne, A., Mohanty, S. and Wopereis, M. C. S. (2012). Crops that feed the world 7: rice. *Food Secur.* **4**, 7-24. doi:10.1007/s12571-012-0168-1
Sengupta, S., Mangu, V., Sanchez, L., Bedre, R., Joshi, R., Rajasekaran, K. and Baisakh, N. (2019). An actin-depolymerizing factor from the halophyte smooth cordgrass, Spartina alterniflora (SaADF2), is superior to its rice homolog (OsADF2) in conferring drought and salt tolerance when constitutively overexpressed in rice. *Plant Biotechnol. J.* **17**, 188-205. doi:10.1111/pbi.12957
Shaner, N. C., Lambert, G. G., Chammas, A., Ni, Y., Cranfill, P. J., Baird, M. A., Sell, B. R., Allen, J. R., Day, R. N., Israelsson, M. et al. (2013). A bright monomeric green fluorescent protein derived from Branchiostoma lanceolatum. *Nat. Methods* **10**, 407-409. doi:10.1038/nmeth.2413
Shaw, S. L., Kamyar, R. and Ehrhardt, D. W. (2003). Sustained microtubule treadmilling in Arabidopsis cortical arrays. *Science* **300**, 1715-1718. doi:10.1126/science.1083529
Sheahan, M. B., Staiger, C. J., Rose, R. J. and McCurdy, D. W. (2004). A green fluorescent protein fusion to actin-binding domain 2 of Arabidopsis fimbrin highlights new features of a dynamic actin cytoskeleton in live plant cells. *Plant Physiol.* **136**, 3968-3978. doi:10.1104/pp.104.049411
Sikora, J., Wasik, A. and Zajaczkowska, M. (1991). Cytoplasmic streaming direction reverses in dividing Paramecium bursaria. *Eur. J. Protistol.* **27**, 352-356. doi:10.1016/S0932-4739(11)80251-8
Song, Y., Li, G., Nowak, J., Zhang, X., Xu, D., Yang, X., Huang, G., Liang, W., Yang, L., Wang, C. et al. (2019). The rice actin-binding protein RMD regulates light-dependent shoot gravitropism. *Plant Physiol.* **181**, 630-644. doi:10.1104/pp.19.00497
Sun, T., Li, S. and Ren, H. (2017). OsFH15, a class I formin, interacts with microfilaments and microtubules to regulate grain size via affecting cell expansion in rice. *Sci. Rep.* **7**, 6538. doi:10.1038/s41598-017-06431-5
Timmers, A. C. J., Vallotton, P., Heym, C. and Menzel, D. (2007). Microtubule dynamics in root hairs of Medicago truncatula. *Eur. J. Cell Biol.* **86**, 69-83. doi:10.1016/j.ejcb.2006.11.001
Ueda, K., Matsuyama, T. and Hashimoto, T. (1999). Visualization of microtubules in living cells of transgenic *Arabidopsis thaliana*. *Protoplasma* **206**, 201-206. doi:10.1007/BF01279267
van der Walt, S., Schönberger, J., Nunez-Iglesias, J., Boulogne, F., Warner, J., Yager, N., Gouillart, E., Yu, T. and scikit-image contributors (2014). scikit-image: image processing in Python. *PeerJ* **2**, e453. doi:10.7717/peerj.453
Vidali, L., Rounds, C. M., Hepler, P. K. and Bezanilla, M. (2009). Lifeact-mEGFP reveals a dynamic apical F-actin network in tip growing plant cells. *PLoS One* **4**, e5744. doi:10.1371/journal.pone.0005744
Wang, X. and Mao, T. (2019). Understanding the functions and mechanisms of plant cytoskeleton in response to environmental signals. *Curr. Opin. Plant Biol.* **52**, 86-96. doi:10.1016/j.pbi.2019.08.002
Wang, M., Chen, C., Xu, Y. Y., Jiang, R. X., Han, Y., Xu, Z. H. and Chong, K. (2004). A practical vector for efficient knockdown of gene expression in rice (Oryza sativa L.). *Plant Mol. Biol. Rep.* **22**, 409-417. doi:10.1007/BF02772683
Wang, C., Li, J. and Yuan, M. (2007). Salt tolerance requires cortical microtubule reorganization in arabidopsis. *Plant Cell Physiol.* **48**, 1534-1547. doi:10.1093/pcp/pcm123
Wang, C., Higgins, J. D., He, Y., Lu, P., Zhang, D. and Liang, W. (2017). Resolvase OsGEN1 mediates DNA repair by homologous recombination. *Plant Physiol.* **173**, 1316-1329. doi:10.1104/pp.16.01726
Wang, L., Qiu, T., Yue, J., Guo, N., He, Y., Han, X., Wang, Q., Jia, P., Wang, H., Li, M. et al. (2021). Arabidopsis ADF1 regulated by MYB73 is involved in response to salt stress via affecting actin filaments organization. *Plant Cell Physiol.* **62**, 1387-1395. doi:10.1093/pcp/pcab081

Xie, K., Minkenberg, B. and Yang, Y. (2015). Boosting CRISPR/Cas9 multiplex editing capability with the endogenous tRNA-processing system. *Proc. Natl. Acad. Sci. USA* **112**, 3570-3575. doi:10.1073/pnas.1420294112

Xu, X. L., Walter, W. J., Liu, Q., Machens, I. and Nick, P. (2018). A rice class-XIV kinesin enters the nucleus in response to cold. *Sci. Rep.* **8**, 3588. doi:10.1038/s41598-018-21816-w

Yang, B. J., Wendrich, J. R., De Rybel, B., Weijers, D. and Xue, H. W. (2020). Rice microtubule-associated protein IQ67-DOMAIN14 regulates grain shape by modulating microtubule cytoskeleton dynamics. *Plant Biotechnol. J.* **18**, 1141-1152. doi:10.1111/pbi.13279

Yu, Y., Wu, S., Nowak, J., Wang, G., Han, L., Feng, Z., Mendrinna, A., Ma, Y., Wang, H., Zhang, X. et al. (2019). Live-cell imaging of the cytoskeleton in elongating cotton fibres. *Nat. Plants* **5**, 498-504. doi:10.1038/s41477-019-0418-8

Zee, S. Y. and Ye, X. L. (2000). Microtubule reorganization during pollen development of rice (Oryza sativa L.). *Protoplasma* **210**, 188-201. doi:10.1007/BF01276859

Zhang, M., Zhang, B., Qian, Q., Yu, Y., Li, R., Zhang, J., Liu, X., Zeng, D., Li, J. and Zhou, Y. (2010). Brittle Culm 12, a dual-targeting kinesin-4 protein, controls cell-cycle progression and wall properties in rice. *Plant J.* **63**, 312-328. doi:10.1111/j.1365-313X.2010.04238.x

Zhang, Z., Zhang, Y., Tan, H., Wang, Y., Li, G., Liang, W., Yuan, Z., Hu, J., Ren, H. and Zhang, D. (2011). RICE MORPHOLOGY DETERMINANT encodes the type II formin FH5 and regulates rice morphogenesis. *Plant Cell* **23**, 681-700. doi:10.1105/tpc.110.081349

Zhang, J., Wang, C., Higgins, J. D., Kim, Y. J., Moon, S., Jung, K. H., Qu, S. and Liang, W. (2019). A multiprotein complex regulates interference-sensitive crossover formation in rice. *Plant Physiol.* **181**, 221-235. doi:10.1104/pp.19.00082

Zhao, Y., Pan, Z., Zhang, Y., Qu, X., Zhang, Y., Yang, Y., Jiang, X., Huang, S., Yuan, M., Schumaker, K. S. et al. (2013). The actin-related Protein2/3 complex regulates mitochondrial-associated calcium signaling during salt stress in Arabidopsis. *Plant Cell* **25**, 4544-4559. doi:10.1105/tpc.113.117887